Journal of Solid State Chemistry 181 (2008) 1434–1438

Contents lists available at ScienceDirect

Journal of Solid State Chemistry

journal homepage: www.elsevier.com/locate/jssc

Preparation and thermoelectric properties of $AgPb_mSbSe_{m+2}$ materials

K.F. Cai [a,*], X.R. He [a], M. Avdeev [b], D.H. Yu [b], J.L. Cui [c], H. Li [a]

[a] Functional Materials Research Laboratory, Tongji University, 1239 Siping Road, Shanghai 200092, China
[b] Bragg Institute, Australian Nuclear Science and Technology Organization, PMB 1, Menai, NSW 2234, Australia
[c] School of Mechanical Engineering, Ningbo University of Technology, Ningbo 315016, China

ARTICLE INFO

Article history:
Received 21 June 2007
Received in revised form
13 March 2008
Accepted 24 March 2008
Available online 26 March 2008

Keywords:
Chalcogenides
Semiconductors
Sintering
Microstructure
Thermoelectric properties

ABSTRACT

Hydrothermally synthesized $AgPb_mSbSe_{m+2}$ ($m = 10$, 12, 16, 18) nanoparticles with diameters of 20–50 nm were compacted by pressureless sintering. The Seebeck coefficient and electrical conductivity of the samples were measured from room temperature up to ~750 K. The samples show large and positive values of the Seebeck coefficient and moderate electrical conductivity. The thermoelectric properties of $Ag_xPb_{18}SbSe_{20}$ ($x = 0.8$, 0.85) and $AgPb_{18}SbSe_{20-y}Te_y$ ($y = 1$, 3) samples have also been studied. It has been found that $Ag_{0.85}Pb_{18}SbSe_{20}$ sample has a higher thermoelectric power factor. A significant difference in thermoelectric properties has also been observed for the $AgPb_{18}SbSe_{20}$ samples prepared with pressureless sintering and spark plasma sintering.

1. Introduction

The effectiveness of a thermoelectric material is determined by a dimensionless thermoelectric figure of merit, $ZT = \alpha^2\sigma T/\kappa$, where α, σ, T and κ are the Seebeck coefficient, electrical conductivity, absolute temperature and thermal conductivity, respectively. In 2004, it was reported that n-type $AgPb_mSbTe_{m+2}$, or LAST-m (LAST for lead, antimony, silver, tellurium) bulk materials exhibited excellent thermoelectric properties. The thermoelectric figure of merit reached 2.1 at 800 K for LAST-18 material [1]. Extensive studies, experimentally and theoretically, on this material system have been stimulated and conducted around the world [2–8] since then. In a series of studies by Kosuga et al. [2–5], relatively poor thermoelectric properties of the system were shown. The best ZT value of about 1.0 at 673 K was obtained for a sample of $Ag_{0.6}Pb_{18}SbTe_{20}$ [4]. Wang et al. [6] studied the system using a combined process of mechanical alloying and spark plasma sintering (SPS). They found that the thermoelectric properties were greatly dependent on the content of Pb. A ZT value of 1.37 at 673 K was obtained for a sample of $Ag_{0.8}Pb_{22}SbTe_{20}$. Hazama et al. [7] have performed first-principle calculations for the LAST-m ($m = 6$, 14 and 30) to clarify the effect of simultaneous doping of Ag and Sb on PbTe. They have concluded that there exists an optimum Ag–Sb concentration, and that the ZT value can be increased beyond that of PbTe at high temperatures around 800 K. Kanatzidis and co-workers carried out *ab initio* electronic structure calculations based on gradient corrected density-functional theory, combined with experimental studies using electron diffraction, powder/single-crystal X-ray diffraction (XRD), high-resolution transmission electron microscopy and atomic pair distribution function [9–11] and found that the materials were unique heterogeneously nanostructured systems. The nanostructures in the materials may be the origin of the large ZT values. Besides the high ZT value of n-type LAST-m materials, they also successfully prepared and studied p-type $Ag_{0.5}Pb_6Sn_2Sb_{0.2}Te_{10}$ with a ZT value of 1.45 at 627 K [12] and p-type $Na_{0.95}Pb_{20}SbTe_{22}$ with a ZT value up to 1.7 at 650 K [13]. Both the materials contain nanostructures. Other studies have also demonstrated the enhancement of the Seebeck coefficient [14–17] or reduction of the thermal conductivity [18,19] due to nanostructures.

In order to reduce material synthesis cost, the Kanatzidis group recently synthesized LAST-m nanoparticles using a reverse micellar approach combined with a sodium borohydride reduction [20]. However, the surface of the synthesized nanoparticles is covered by a layer of organic material that has to be removed before compacting and obviously it is a hard nut to crack.

PbSe is an analogue of PbTe; therefore $AgPb_mSbSe_{m+2}$ or LASS-m (LASS for lead, antimony, silver, selenium) is expected to have similar properties to those of the LAST-m system. We have successfully synthesized LASS-m nanopowders via a hydrothermal synthesis method [21], which can also be used to synthesize LAST-m nanopowders. Unlike the nanoparticles synthesized in Ref. [20], the hydrothermally synthesized nanopowders can be

* Corresponding author. Fax: +86 21 65980255.
E-mail address: kfcai@mail.tongji.edu.cn (K.F. Cai).

0022-4596/$ - see front matter © 2008 Elsevier Inc. All rights reserved.
doi:10.1016/j.jssc.2008.03.018

directly used for sintering. In this paper, we report systematic studies on a series of hydrothermally synthesized LASS-*m* nanopowders in a compacted form by pressureless sintering (PS) and/or SPS. The thermoelectric properties of the sintered sample were measured from room temperature up to 750 K. The structure of the materials has been studied by scanning electron microscopy (SEM) and XRD.

2. Experimental procedure

Three kinds of nanopowders of $AgPb_mSbSe_{m+2}$ (LASS-*m* with $m = 10, 12, 16, 18$), $Ag_xPb_{18}SbSe_{20}$ ($x = 0.8, 0.85$) and $AgPb_{18}SbSe_{20-y}Te_y$ ($y = 1, 3$) were hydrothermally synthesized at 180 °C for 20 h. The starting materials are selenium powder, lead nitrate, silver nitrate and antimony nitrate with $NaBH_4$ as a reductant. The size of the nanopowders is in the range of 20–50 nm and most nanopowders are 35 nm in size. The detailed method can be referred to in Ref. [21].

The synthesized nanopowders were uniaxially pressed into pellets (12 mm in diameter and 1 mm thick). The pellets were heated to 620 °C in Ar flowing at 6 ml/min in a quartz tube furnace and held at this temperature for 30 min. The pellets were then cooled down to 580 °C in 40 min and held at 580 °C for 300 min before being cooled down to 300 °C in 280 min followed by natural cooling down to room temperature. For comparison, $Ag_{0.85}Pb_{18}SbSe_{20}$ nanopowder was also sintered by SPS in a graphite die at 560 °C, under 40 MPa pressure for 1 min in vacuum with a heating rate of 40 °C/min. The real sintering temperature at sample for SPS could be a few tens of degrees higher as the thermocouple was attached at the graphite die only. The density of the sintered samples was determined by the water displacement method. The sintered samples were examined by XRD and SEM. The samples were cut into small rectangular ($10 \times 1 \times 2\,mm^3$) pieces for thermoelectric properties measurement. Electrical conductivity and Seebeck coefficient measurements were carried out by using a computer-controlled testing system up to about 750 K under argon atmosphere. Electrical conductivity measurements were performed using a steady-state four-probe technique with chopped direct current (~10 mA). The Seebeck coefficient was determined by the slope of the linear relationship between the thermal electromotive force and temperature difference (10–15 K) between the two ends of the sample. The error of the measured Seebeck coefficient was about 10%. The Hall coefficient and carrier concentration of the samples were measured using HMS-3000 at room temperature.

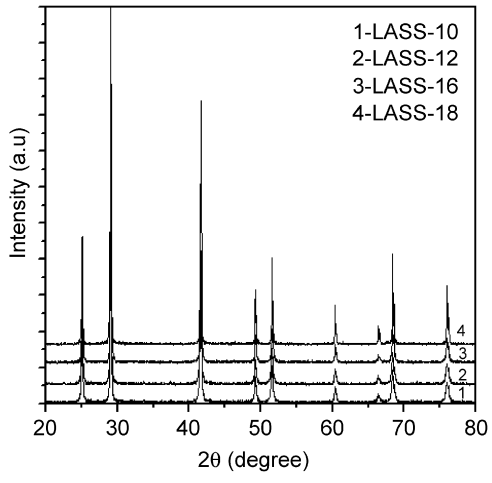

Fig. 1. XRD patterns for the LASS-*m* ($m = 10, 12, 16, 18$) samples.

3. Results and discussion

The bulk densities of all the samples are ~92% of the theoretical values. The effect of porosity on the thermoelectric properties is neglected in the following discussions. XRD analysis reveals that all the sintered samples have PbSe structure with no impurity phases, as shown in Fig. 1 for the LASS-*m* ($m = 10, 12, 16, 18$) samples. The carrier concentration and Hall coefficient of some samples are given in Table 1. As seen in the Table 1, the carrier concentration increases with decreasing *m* value in the LASS-*m* samples and decreasing *x* value in the $Ag_xPb_{18}SbSe_{20}$ ($x = 0.85, 1$) samples. However, increasing the *y* value increases the carrier concentration in the $AgPb_{18}SbSe_{20-y}Te_y$ ($y = 0, 1, 3$) samples.

Figs. 2(a) and (b) are the temperature dependence of electrical conductivity and Seebeck coefficient, respectively, for the pressureless sintered LASS-*m* samples. It is seen from Fig. 2(a) that the electrical conductivity of all the samples increases to a peak value and then decreases with temperature. The temperatures corresponding to the peak values change slightly from 460 to 480 K. The observed temperature dependence before the peak values indicates semiconducting behavior. Fig. 2(b) shows that the Seebeck coefficient of all the samples increases with temperature and reaches a peak value at around 650 K followed by a gradual decrease. At a given temperature, the electrical conductivity of the samples decreases with the increase of *m* values, whereas the Seebeck coefficient shows opposite tendency. The positive values of the Seebeck coefficient are observed in the whole temperature range, indicating p-type conduction.

Figs. 3(a) and (b) show the temperature dependence of electrical conductivity and Seebeck coefficient for the $Ag_xPb_{18}SbSe_{20}$ ($x = 0.8, 0.85, 1$) samples. It is seen from Fig. 3(a) that the change of Ag content significantly affects the thermoelectric properties. The $Ag_{0.85}Pb_{18}SbSe_{20}$ sample has the highest electrical conductivity among the three samples. Similar Seebeck coefficients are obtained for the samples with $x = 0.8$ and 0.85, while the sample with $x = 1$ gives higher Seebeck coefficient at higher temperatures as indicated in Fig. 3(b). However, the sample with $x = 0.85$ has achieved the highest power factors ($\sim 6 \times 10^{-4}$ W/mK^2 at 470 K) among these three samples.

Figs. 4(a) and (b) show the temperature dependence of electrical conductivity and Seebeck coefficient of the $AgPb_{18}SbSe_{20-y}Te_y$ ($y = 0, 1, 3$) samples. As indicated in Fig. 4(a), the Te-doped samples exhibit higher electrical conductivity than the undoped sample. The peak position of electrical conductivity for $AgPb_{18}SbSe_{19}Te$ sample shifts to a higher temperature (~530 K) as compared with the undoped sample. When temperature is below 450 K, the electrical conductivity for the two Te-doped samples is similar. When the temperature is above 450 K, the electrical

Table 1
Some physical properties of the samples

Sample	Lass-10	Lass-12	Lass-16	Lass-18	$Ag_{0.85}Pb_{18}SbSe_{20}$	$AgPb_{18}SbSe_{19}Te$	$AgPb_{18}SbSe_{17}Te_3$
Hall coefficient 10^{-2} (cm^3C^{-1})	7.866	10.55	33.44	33.72	17.8	32.73	31.26
Carrier concentration 10^{19} (cm^{-3})	7.936	5.919	1.866	1.851	3.492	1.907	1.997

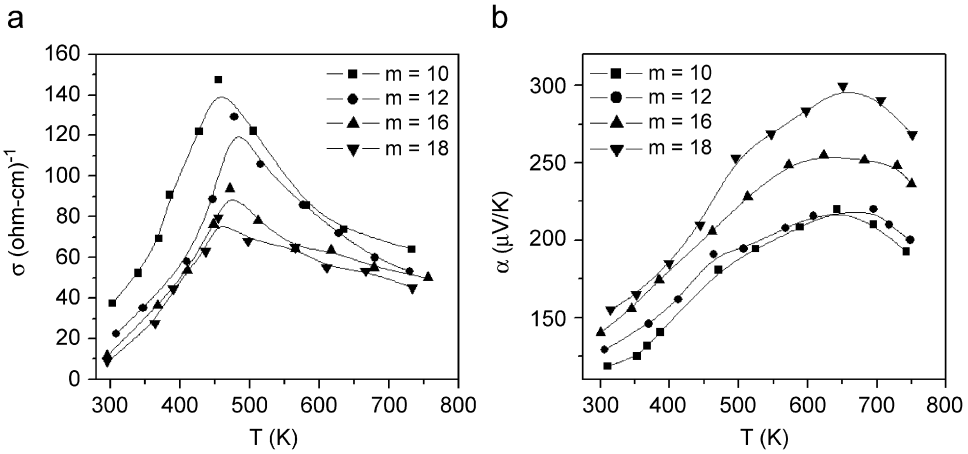

Fig. 2. Temperature dependence of electrical conductivity (a) and Seebeck coefficient (b) of the pressureless sintered LASS-*m* samples.

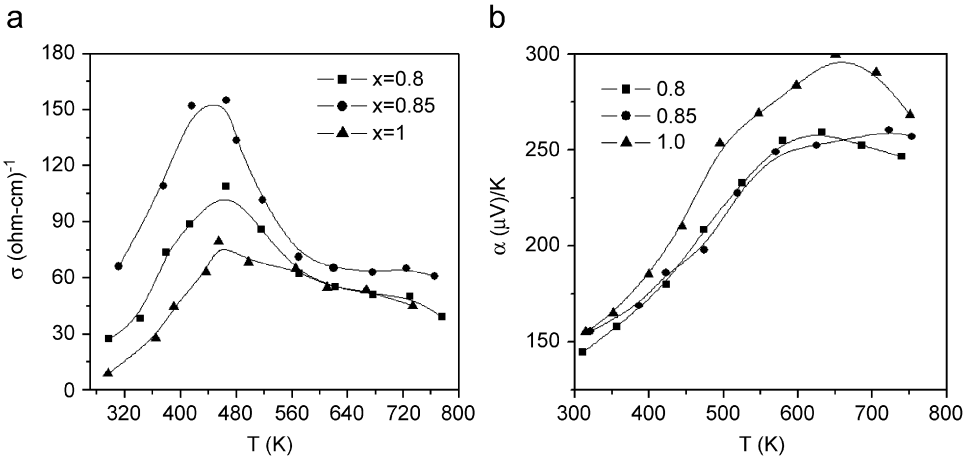

Fig. 3. Temperature dependence of electrical conductivity (a) and Seebeck coefficient (b) of the pressureless sintered $Ag_xPb_{18}SbSe_{20}$ ($x = 0.8, 0.85, 1$) samples.

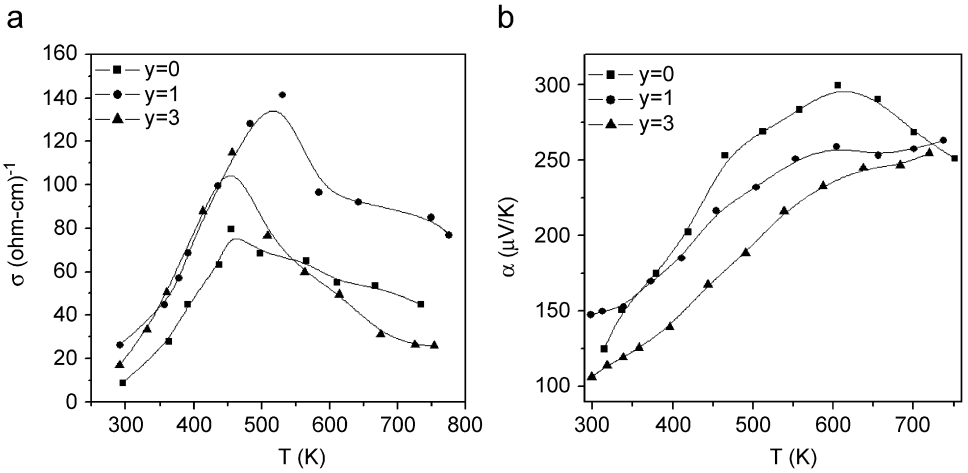

Fig. 4. Temperature dependence of electrical conductivity (a) and Seebeck coefficient (b) of the pressureless sintered $AgPb_{18}SbSe_{20-y}Te_y$ ($y = 0, 1, 3$) samples.

conductivity for the $AgPb_{18}SbSe_{17}Te_3$ sample is less than that for the $AgPb_{18}SbSe_{19}Te$ sample. When the temperature is above 550 K, the electrical conductivity for the $AgPb_{18}SbSe_{17}Te_3$ sample is even lower than that for the undoped sample ($AgPb_{18}SbSe_{20}$). Doping Te decreases the Seebeck coefficient as shown in Fig. 4(b).

Electrical conductivity of a material is proportional to its carrier concentration. The electrical conductivity of the above-mentioned samples, apart from the $AgPb_{18}SbSe_{17}Te_3$ sample, is consistent with the carrier concentration results given in Table 1. For the $AgPb_{18}SbSe_{17}Te_3$ sample, there may be some elemental Te presented in the sample and this may cause a relative low

electrical conductivity. The experiment indicates that an optimal Te doping level exists.

If we assume a Boltzmann distribution for the carriers (holes), the Seebeck coefficient will decrease as the carrier concentration increases [22]. As shown in Figs. 2(b), 3(b) and 4(b), the Seebeck coefficient of the samples decreases with decreasing m value in the LASS-m samples and decreasing x value in the $Ag_xPb_{18}SbSe_{20}$ ($x = 0.85, 1$) samples, while it decreases with increasing y value in the $AgPb_{18}SbSe_{20-y}Te_y$ ($y = 0,\ 1,\ 3$) samples. These trends are perfectly consistent with the concentration change as presented in Table 1.

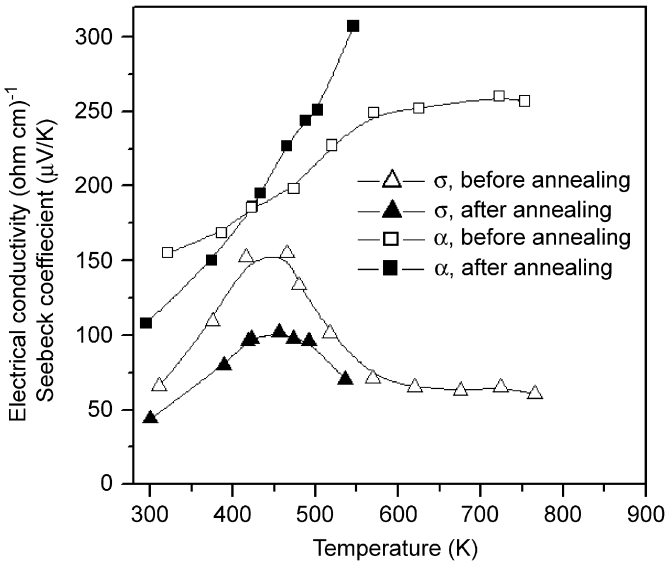

Fig. 5. Electrical transport properties before and after annealing for the pressureless sintered $Ag_{0.85}Pb_{18}SbSe_{20}$ sample.

It is necessary to make further clarifications on the temperature dependence observed in the electrical conductivity and Seebeck coefficient, as displayed in Figs. 2(a) and (b). We have observed that the electrical conductivity of most of the above-mentioned samples changes temperature dependence at around 460–480 K. This phenomenon may reflect the changes of the structure and/or composition of the materials as a function of temperature.

To see whether there is a change in structure as a function of temperature, we performed XRD as a function of temperature from room temperature to 773 K on the LASS-10 nanopowder. The XRD patterns show that all the peaks can be indexed to PbSe (JCPDS card no. 77-0245) independent of temperature. Since no new phase is observed from the temperature-dependent XRD patterns, the observed temperature dependence in the electrical conductivity should be due to composition change. When we synthesized the LASS-10 nanopowders, we noticed that as the synthesis temperature was lower then 180 °C or the holding time at 180 °C was less than 20 h, some unreacted Se remained in the powder. Therefore, the as-synthesized powders may also contain unreacted Se, whose content is lower than the resolution of XRD performed but high enough to affect the conductivity and Seebeck coefficient of the samples. In fact we did observe that a thin red film appeared at the upper inner wall at the outlet end of the quartz tube during the PS process. A similar film was also observed on the chamber of the testing system after several runs in the measurements of the thermoelectric properties of these samples. We believe that the film is amorphous Se resulting from the volatilization of unreacted Se [23].

In order to further confirm that there is a change in composition as a function of temperature, the $Ag_{0.85}Pb_{18}SbSe_{20}$

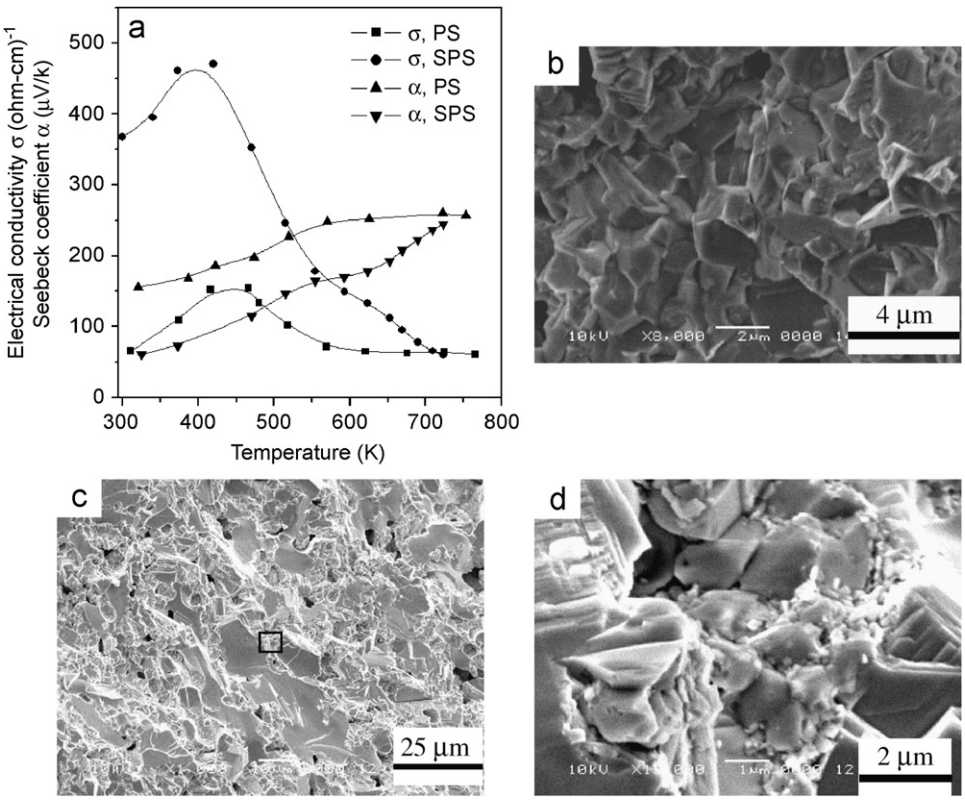

Fig. 6. (a) Temperature dependence of electrical conductivity and Seebeck coefficient of the $Ag_{0.85}Pb_{18}SbSe_{20}$ samples compacted by PS and SPS; SEM images of the fracture surface of the $Ag_{0.85}Pb_{18}SbSe_{20}$ samples compacted by (b) PS and (c) SPS; (d) high magnification image of the black square area indicated in (c).

sample was annealed at 550 K for 48 h and its electrical transport properties were measured. Fig. 5 shows the electrical transport properties of the $Ag_{0.85}Pb_{18}SbSe_{20}$ sample before and after annealing. It can be seen that the electrical conductivity of the annealed sample is lower than that of the sample before annealing at a given temperature. The change of electrical conductivity with temperature becomes slow after annealing. However, the Seebeck coefficient increases more quickly with temperature after annealing. These changes should be related to the reduction of unreacted Se in the sample.

Fig. 6(a) shows the effects from different sintering processes (PS and SPS) on electrical conductivity and Seebeck coefficient. It can be seen from Fig. 6(a) that different sintering processes have significant influence on the thermoelectric properties. However, the electrical conductivity and Seebeck coefficient of both samples change in a similar way with temperature. The electrical conductivity of the SPS sample is much higher than that of the PS sample except at high temperature (~720 K) when the electrical conductivities of the two samples merge. Like the electrical conductivity, the Seebeck coefficients of the two samples tend to converge to a common value at high temperature (~750 K).

Figs. 6(b) and (c) show the SEM images of the fracture surface of the $Ag_{0.85}Pb_{18}SbSe_{20}$ samples compacted by PS and SPS, respectively. The microstructure of all other pressureless sintered samples is similar to that shown in Fig. 6(b). As indicated in the figures, the pressureless sintered sample is homogeneous and the grains are fine with diameter $<2\,\mu m$. The spark plasma sintered sample has two main grain sizes: bigger ($>10\,\mu m$) and smaller (about 100–200 nm). The different grain sizes can be clearly seen from the magnified SEM image (corresponding to the zone marked by a black square in Fig. 6(c)) as shown in Fig. 6(d). Thus a composite with a mixture of nano- and microstructure can be produced by SPS.

The PS process can be achieved under a nearly thermal equilibrium condition due to an ambient heating source, whereas the SPS technique does not necessarily happen under equilibrium condition due to non-uniform heating from the electrical current flowing through the sample and the graphite die [24]. This may cause very different microstructures between the PS and SPS samples. In addition, due to a fast heating rate and an additional pressure applied in the SPS process, the volatilization of unreacted Se could be much depressed as compared with the PS process, and this could also cause the SPS sample with unusual microstructure. Thus the different sintering methods could introduce different compositions and microstructures in the samples and consequently cause the different thermoelectric properties.

4. Conclusions

The microstructure and thermoelectric properties of pressureless sintered LASS-*m* samples have been studied. The samples show p-type conducting behavior. Slightly decreasing the amount of Ag in LASS-18 significantly increases the electrical conductivity and decreases somewhat the Seebeck coefficient. The $Ag_{0.85}Pb_{18}SbSe_{20}$ sample has better thermoelectric properties. The power factor of the $Ag_{0.85}Pb_{18}SbSe_{20}$ sample is about $6\times10^{-4}\,W/mK^2$ at 470 K. Doping a suitable amount of Te can also improve the thermoelectric properties of the LASS-18 sample. The different electrical transport properties from PS and SPS samples are mainly due to differences in microstructure and composition. The studies indicated that the SPS process could produce composite materials with a mixture of nano/microstructures. Such kind of LASS-*m* thermoelectric materials may show better thermoelectric properties if the composition is further optimized, since the large grains can provide good electrical conductivity and the nanograins can scatter phonons to provide low thermal conductivity.

Acknowledgments

This work was supported by the Science and Technology Commission of Shanghai Municipality (05ZR14124), Shanghai Pujiang Program and 973 Program (2007CB607500).

References

[1] K.F. Hsu, S. Loo, F. Gou, W. Chen, J.S. Dyck, C. Uher, T. Hogan, E.K. Polychroniadis, M.G. Kanatzdis, Science 303 (2004) 818–821.
[2] A. Kosuga, M. Uno, K. Kurosaki, S. Yamanaka, J. Alloys Compd. 387 (2005) 52–55.
[3] A. Kosuga, K. Kurosaki, M. Uno, S. Yamanaka, J. Alloys Compd. 386 (2005) 315–318.
[4] A. Kosuga, M. Uno, K. Kurosaki, S. Yamanaka, J. Alloys Compd. 391 (2005) 288–291.
[5] A. Kosuga, K. Kurosaki, H. Muta, S. Yamanaka, J. Alloys Compd. 416 (2006) 218–221.
[6] H. Wang, J.F. Li, C.W. Nan, M. Zhou, W.S. Liu, B.P. Zhang, T. Kita, Appl. Phys. Lett. 88 (2006) 092104–092106.
[7] H. Hazama, U. Mizutani, R. Asahi, Phys. Rev. B 73 (2006) 115108–115112.
[8] N. Chen, F. Gascoin, G.J. Snyder, E. Müller, G. karpinski, C. Stiewe, Appl. Phys. Lett. 87 (2005) 171903–171905.
[9] D. Bilc, S.D. Mahanti, E. Quarez, K.F. Hsu, R. Pcionck, M.G. Kanatzidis, Phys. Rev. Lett. 93 (2004) 146403-1–146403-4.
[10] E. Quarez, K.F. Hsu, R. Pcionek, N. Frangis, E.K. Polychroniadis, M.G. Kanatzidis, J. Am. Chem. Soc. 127 (2005) 9177–9190.
[11] H. Lin, E.S. Bozin, S.J.L. Billinge, et al., Phys. Rev. B 72 (2005) 174113–174117.
[12] J. Androulakis, K.F. Hsu, R. Pcionek, H. Kong, C. Uher, J.J. D'Angelo, A. Downey, T. Hogan, M.G. Kanatzidis, Adv. Mater. 18 (2006) 1170–1173.
[13] P.F.P. Poudeu, J.D. Angelo, A.D. Downey, J.L. Short, T.P. Hogan, M.G. Kanatzidis, Angew. Chem. Int. Ed. 45 (2006) 3835–3838.
[14] J.P. Heremans, C.M. Thrush, D.T. Morelli, Phys. Rev. B 70 (2004) 115334-1–115334-5.
[15] J.P. Heremans, C.M. Thrush, D.T. Morelli, J. Appl. Phys. 98 (2005) 063703–063706.
[16] T.C. Harman, P.J. Tayler, M.P. Walsh, B.E. LaForge, Science 297 (2002) 2229–2232.
[17] J.P. Heremans, C.M. Thrush, D.T. Morelli, M.C. Wu, Phys. Rev. Lett. 88 (2002) 216801-1–216801-5.
[18] D.G. Cahill, W.K. Ford, K.E. Goodson, G.D. Mahan, A. Majumdar, H.J. Maris, R. Merlin, S.R. Phillpot, J. Appl. Phys. 93 (2003) 793–796.
[19] R. Venkatasubramanian, E. Siivola, T. Colpitts, B. O'Quinn, Nature (London) 413 (2001) 597–601.
[20] A.J. Karkamkar, M.G. Kanatzdis, J. Am. Chem. Soc. 128 (2006) 6002–6004.
[21] K.F. Cai, X.R. He, Mater. Lett. 60 (2006) 2461–2464.
[22] S.S. Kim, S. Yamamoto, T. Aizawa, J. Alloys Compd. 375 (2004) 107–113.
[23] E.A. Dalchiele, S. Cattarin, M.M. Musiani, J.Appl. Electrochem. 28 (1998) 1005–1009.
[24] T. Noguchi, in: Proceedings of the 16th International Conference on Thermoelectrics, IEEE, Dresden, 1997, pp. 207–214.